Femtosecond-pulse two-photon resonant difference-frequency mixing in gases: A technique for tunable vacuum-ultraviolet femtosecond-pulse generation and a spectroscopic tool for studying atoms in strong laser fields

A. Nazarkin,* G. Korn, O. Kittelmann, J. Ringling, and I. V. Hertel
Max-Born-Institut für Nichtlineare Optik und Kurzzeitspektroskopie, Rudower Chaussee 6, D-12489 Berlin, Germany
(Received 29 October 1996)

Two-photon resonant and near-resonant four-wave difference-frequency mixing in gases in the interaction regime when laser pulse durations are comparable to or shorter than the medium polarization relaxation time T_2' is investigated. The results of experimental studies of the process in Ar and Kr using pump pulses from the ArF-excimer laser are presented demonstrating a generation of tunable short pulse radiation in the range 102–124 nm. The results are discussed in terms of a theoretical model based on a self-consistent solution of the Bloch equations for the atomic transitions and the Maxwell equations for the fields. This enables one to interpret specific nonstationary resonant and quasiresonant phenomena involved in the frequency conversion process. It is shown that the femtosecond-pulse four-wave frequency-mixing technique with probe pulses significantly shorter than the pump pulses makes it possible to study the coherent dynamics of an atomic transition exposed to an intense field. Using atomic Kr as the nonlinear medium, coherent Rabi oscillations and the subsequent phase relaxation of excitation were observed under the condition of two-photon interaction of Kr with femtosecond 193-nm laser pulses. The obtained information is important for controlling and optimizing processes of two-photon resonant frequency conversion and for time-resolved studies of Rydberg states in atoms and molecules. [S1050-2947(97)08406-0]

PACS number(s): 42.50.Hz, 42.50.Md, 42.65.Ky, 42.65.Hw

INTRODUCTION

Time-resolved spectroscopic studies of ultrafast processes at surfaces or in gaseous media, e.g., photodissociation and fragmentation of molecules and clusters [1], require femtosecond pulses tunable in the vacuum ultraviolet (vuv) spectral range. Because of absorption and phasematching constraints, the generation of tunable femtosecond vuv radiation by cascaded second-order frequency mixing in solid-state nonlinear optical materials is restricted [2] to wavelengths of about 170 nm. On the other hand, third-order frequency mixing schemes pumped by high brightness uv laser systems have the potential to produce coherent radiation in the vuv and soft-x-ray region, which has been demonstrated already for nanosecond pulses [3].

Among the third-order frequency mixing schemes, the scheme of four-wave difference-frequency mixing (FWDFM)

$$\omega_3 = 2\omega_1 - \omega_2, \tag{1}$$

where ω_1 is the pump pulse frequency and ω_2 is the frequency of the injected pulse, is experimentally most preferable. While sum-frequency mixing is restricted to spectral regions of negative dispersion, scheme (1) is possible for both negative and positive dispersion regions of the nonlinear medium [4]. Nonresonant difference-frequency schemes have been shown to have low conversion efficiencies, typically in the range 10^{-5}–10^{-6} for input powers of 1–5 MW [5]. However, if the pump pulse frequency ω_1 is tuned to a resonance with a two-photon transition, i.e., $2\omega_1 \approx \omega_{21}$, a large enhancement in conversion efficiency can be achieved. Recently it has been demonstrated that the process of vuv generation employing near-resonant two-photon FWDF schemes, Eq. (1), in noble gases pumped by intense femtosecond pulses from KrF and ArF lasers (ω_1) and additional injected laser pulses (ω_2) can provide conversion efficiencies as high as several percent [6–9], and therefore is of considerable practical importance.

From the fundamental viewpoint, the processes of femtosecond pulse two-photon resonant frequency conversion bear a number of interesting physical features which could not be observed with picosecond and even less with nanosecond pulses. This is due to the fact that for laser pulses of femtosecond duration the condition

$$\tau_p < T_2' \tag{2}$$

(where T_2' is the irreversible polarization relaxation time of the medium) can be easily fulfilled, and the effects of coherent interaction between the pulse and atomic medium come into play. The characteristic feature of coherent interaction is that the medium response to a resonant field is no longer determined by the instantaneous value of the field amplitude and phase, but depends on the pulse amplitude and phase in all preceding moments of the radiation-matter interaction (coherent memory effect). Under these conditions, such coherent phenomena as Rabi oscillations of atomic transition populations, self-induced transparency, breakup of intense pulses into subpulses, etc., have been theoretically predicted [10]. Although many aspects of frequency conversion in the regime of coherent interaction have been understood theoretically in the early 1980s [11–13], a progress in experi-

*Permanent address: P. N. Lebedev Physical Institute of the Russian Academy of Sciences, Leninsky Prospect 53, 117924 Moscow, Russia.

mental studies of these processes has been made only with the development of high-power solid-state and excimer laser systems producing nearly bandwidth-limited femtosecond pulses [6–9]. In order to explain experimental results on FWDFM the traditional nonlinear susceptibility approach is commonly used. However, the approach turns out to be ineffective in description of nonlinear optical processes specific to the regime of resonant and quasiresonant frequency conversion, and therefore an adequate theoretical analysis of femtosecond-pulse FWDFG is needed. Particularly, the analysis should answer such questions as: what are the characteristics of quasiresonant and resonant conversion with intense femtosecond pulses, and what are the maximum achievable conversion efficiencies for these processes?

The technique of two-photon resonant four-wave mixing with intense pump pulses (ω_1) and relatively week injected (probe) (ω_2) pulses represents a very powerful tools for spectroscopic study of ultrafast processes in solids, liquids and gases [14,15]. However, until now the technique has mainly been used for studies of the temporal evolution of a quantum system after it was excited by an intense pump pulse, and to our knowledge has never been employed to study the dynamics of radiation-matter interaction itself. Recently, it was shown experimentally that the use of probe pulses significantly shorter than pump pulses opens up the possibility to investigate directly coherent dynamics of quantum transitions in a strong laser field [9].

In this paper we present the results of experimental and theoretical studies of difference-frequency generation under the condition of resonant and near-resonant excitation of atomic Kr and Ar by femtosecond pulses. We report on the generation of femtosecond vuv radiation tunable between 102–124 nm using intense ultrashort ArF pump pulses and tunable synchronized femtosecond output pulses of an optical parametric generator. A detailed theoretical analysis of the physical processes involved in FWDFM is presented. We also demonstrate that the developed experimental technique enables the observation of two-photon Rabi oscillations in atomic Kr which is extremely important for optimization of the FWDFM process. The paper is organized as follows. In Sec. I the general theoretical approach based on a self-consistent solution of the Maxwell-Bloch equations for the interacting fields and a two-photon resonant medium is developed, and the maximum achievable conversion efficiencies for quasiresonant and on-resonant FWDFM are analyzed. In Sec. II the arrangement used for generation of the difference-frequency radiation is described. Experimental results on tunable vuv pulse generation in Ar and Kr and their discussion are presented in Sec. III. In Sec. IV the applications of four-wave frequency mixing with femtosecond pulses to a study of an atom in a strong laser field are discussed, and experimental results on the coherent dynamics of the two-photon transition of atomic Kr are presented.

I. THEORETICAL APPROACH

Experimental results on FWDFM in gases with intense femtosecond pulses are usually discussed using formulas of traditional theory of nonlinear susceptibility (see, for example, [16,17]). The corresponding expressions for the generated field are derived under the assumptions that the carrier frequencies of interacting fields lie far from resonances with atomic transitions, and that the medium polarization can be represented as a power expansion with a small parameter. In this way one can roughly estimate the order of magnitude of the nonlinear polarizability of the medium, but the approach turns out to be ineffective in the description of many specific features of quasiresonant and even less of resonant femtosecond-pulse frequency conversion such as time-dependent medium response and nonstationary excitation of atomic levels, the dynamical Stark shift of the transition frequency in a strong laser field, saturation effects, etc. which have been recently observed in femtosecond-pulse experiments [6–8,18].

A number of physical factors play a role when femtosecond pulses with a carrier frequency close to a two-photon resonance with an atomic transition and intensity level of several TW/cm^2 are used in FWDFM experiments. First, on the femtosecond time scale, condition (2) can be easily realized and specific nonlinear effects, such as Rabi nutation of atomic populations, coherent propagation phenomena, etc. [10–13], can have a strong influence on the FWDFM process. A further important feature of resonantly enhanced FWDFM lies in the fact that both the pump field photons and the generated and the injected field photons are resonant to the two-photon atomic transition: $\omega_1+\omega_1=\omega_2+\omega_3\approx\omega_{12}$. As a consequence, a counteraction of the two resonant two-photon processes occurs which leads to a saturation of frequency conversion even in the case of ideal phase matching. The above factors are dominating at the nonlinear stage of FWDFM and, consequently, an analysis of this stage would be of prime importance from the viewpoint of maximum achievable conversion efficiencies.

Thus the goal of the present theoretical analysis is to elucidate the limiting characteristics of near-resonant and resonant FWDFM for pulses short compared to the polarization relaxation time T_2, and to determine the corresponding optimum parameters of the pump and the injected field. [Relevant schemes of FWDFM in atomic Ar and Kr are shown in Figs. 1(a) and 1(b)].

A. Basic equations

In order to describe the process of femtosecond-pulse FWDFM adequately, we start from a general approach based on the self-consistent solution of the Maxwell equations for the interacting fields and the density-matrix equations for the resonant atoms. The approach has already been applied to a study of ultrashort-pulse two-photon resonant third-harmonic generation in gases and vapors [12,13]. Following this approach, we consider the interaction of a forbidden atomic transition of a frequency ω_{21} with collinearly propagating quasimonochromatic laser fields $e_i(z,t)=\frac{1}{2}\{E_i(z,t)\exp[i(\omega_i t-k_i z]+\text{c.c.}\}$, with carrier frequencies ω_i $(i=1,2,3)$ satisfying the resonance condition $2\omega_1=\omega_2+\omega_3\approx\omega_{21}$. Using the standard density-matrix formalism and the rotating-wave approximation [10], one can derive the following equations (Bloch equations) for the density-matrix elements σ_{ij} $(i,j=1,2)$ of the transition

$$\frac{\partial\sigma_{12}}{\partial\tau}=i\Delta\Omega\sigma_{12}-in\left\{\frac{r_{12}}{4\hbar}(E_1^*)^2+\frac{q_{12}}{4\hbar}(E_2E_3)^*e^{-i\Delta kz}\right\}$$

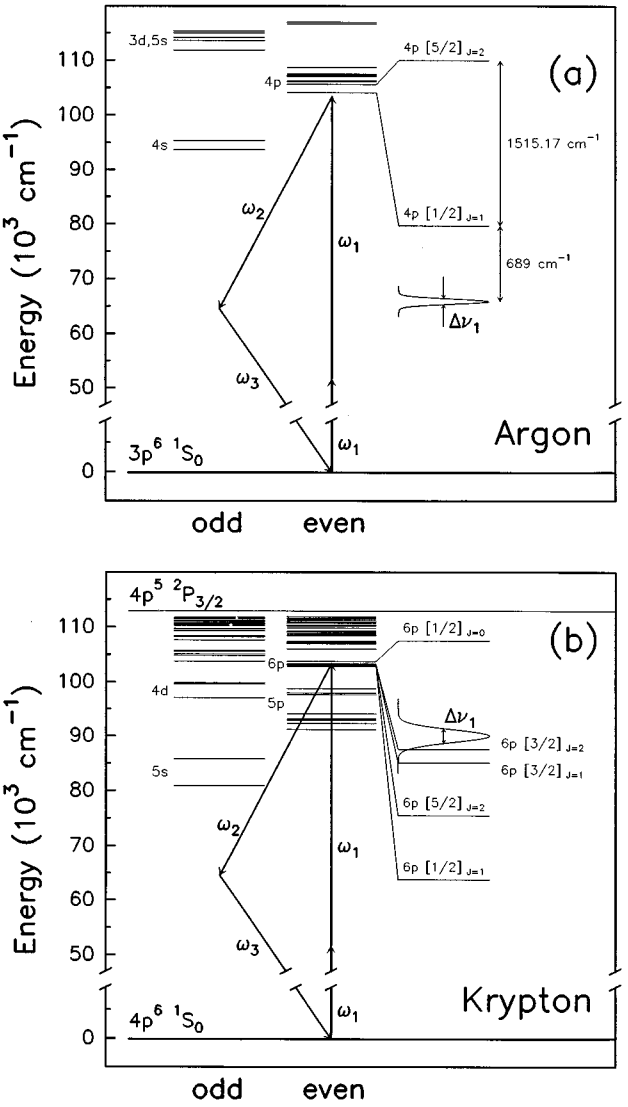

FIG. 1. Relevant scheme of two-photon resonant difference-frequency generation in atomic argon (a) and krypton (b): ω_1, the pump field frequency; ω_2, the injected field frequency; ω_3, the generated field frequency.

$$-\frac{\sigma_{12}}{T_2}, \tag{3a}$$

$$\frac{\partial n}{\partial \tau}=4\,\mathrm{Im}\left\{\left(\frac{r_{12}}{4\hbar}E_1^2+\frac{q_{12}}{4\hbar}E_2E_3e^{i\Delta kz}\right)\sigma_{12}\right\}-\frac{n-1}{T_1}, \tag{3b}$$

where $n=(\sigma_{22}-\sigma_{11})$ is the population difference of the two levels, and T_1 and T_2' are the phenomenological relaxation times for the population difference n and for the density matrix off-diagonal element σ_{12} (below we name σ_{12} ''two-photon excitation''), respectively.

The coupling between the pump field E_1 and the resonant transition is characterized by the two-photon matrix element

$$r_{12}=\hbar^{-1}\sum_m \mu_{2m}\mu_{m1}\left(\frac{1}{\omega_{m1}-\omega_1}\right), \tag{4}$$

where ω_{ij} and μ_{ij} are the frequency and the dipole moment of the transition $i\rightarrow j$, respectively, and the summation in Eq. (4) is made over all the intermediate states m with $m\neq 1$ and 2.

The corresponding matrix element for the process of emission (absorption) of two photons $\hbar\omega_2$ and $\hbar\omega_3$ is given by

$$q_{12}=\hbar^{-1}\sum_m \mu_{2m}\mu_{m1}\left(\frac{1}{\omega_{m1}-\omega_3}+\frac{1}{\omega_{m1}-\omega_2}\right). \tag{5}$$

The full frequency detuning $\Delta\Omega$ entering Eqs. (3) consists of the detuning $\Delta\omega$ of the pump field from the resonant frequency ω_{21} and the dynamical Stark shift $\Delta\omega_{\mathrm{St}}(t)$ of the transition frequency, which is induced by the fields:

$$\Delta\Omega=\Delta\omega+\Delta\omega_{\mathrm{St}}=(2\omega_1-\omega_{21})+\frac{1}{4\hbar}\sum_{i=1}^{3}(\alpha_{22}^{(i)}-\alpha_{11}^{(i)})|E_i|^2, \tag{6}$$

with $\alpha_{11}^{(i)}$ and $\alpha_{22}^{(i)}$ being the linear polarizabilities of levels 1 and 2 at frequency ω_i.

The phase factor Δkz in Eqs. (3) arises from a nonresonant contribution into the wave-number mismatch (for example, due to an addition of a buffer gas) $\Delta k=2k_1-k_2-k_3$. The full wave-number mismatch contains, in addition to the nonresonant contribution, the resonant one determined by the polarizabilities and populations of the levels (see below).

The material equations (3) should be supplemented by the initial conditions

$$\sigma_{12}(z,-\infty)=0,\quad n(z,-\infty)=-1, \tag{7}$$

implying that before the interaction with the fields ($\tau\rightarrow-\infty$) all atoms occupy the ground level.

In the plane-wave approximation the Maxwell equations can be reduced to the following set of equations for slowly varying complex amplitudes of the fields:

$$\frac{\partial E_1}{\partial z}=-i\left(\frac{2\pi\omega_1N}{c}\right)[(\sigma_{11}\alpha_{11}^{(1)}+\sigma_{22}\alpha_{22}^{(1)})E_1+2r_{12}E_1^*\sigma_{12}^*], \tag{8a}$$

$$\frac{\partial E_2}{\partial z}=-i\left(\frac{2\pi\omega_2N}{c}\right)[(\sigma_{11}\alpha_{11}^{(2)}+\sigma_{22}\alpha_{22}^{(2)})E_2+q_{12}E_3^*\sigma_{12}^*], \tag{8b}$$

$$\frac{\partial E_3}{\partial z}=-i\left(\frac{2\pi\omega_3N}{c}\right)[(\sigma_{11}\alpha_{11}^{(3)}+\sigma_{22}\alpha_{22}^{(3)})E_3+q_{12}E_2^*\sigma_{12}^*], \tag{8c}$$

where N is the density number of resonant atoms. In Eqs. (8) we neglect the linear dispersion of group velocities of the pulses by putting $v_1=v_2=v_3=c$. Although this is not the case for short-pulse frequency conversion in solids, the condition can be met in not-too-dense gaseous media [5]. This allowed us to use, in Eqs. (8), the retarded coordinate system $(z,t)\rightarrow[z,\tau=(t-z/c)]$. The boundary conditions at $z=0$ then can be written as $E_1(0,\tau)=E_1(\tau)$, $E_2(0,\tau)=E_2(\tau)$, and $E_3(0,\tau)=0$.

The system of Maxwell-Bloch equations (3)–(8) can be generalized to account for the processes of medium ionization by the fields which can be important in the conditions of on-resonant FWDFM. As was shown in [12], one-photon ionization of an atom from the resonant levels is automatically included in the theory by considering the polarizabilities of the levels to be complex quantities. We discuss the influence of photoionization on FWDFM in more detail in Sec. IV of this paper, in connection with resonant FWDFM experiments.

From the Maxwell equations (8) for the fields, it follows that the difference in the number of photons in the injected (E_2) and the generated (E_3) field is kept constant during the interaction,

$$\frac{|E_2(z,\tau)|^2}{\hbar\omega_2}-\frac{|E_3(z,\tau)|^2}{\hbar\omega_3}=\frac{|E_2(z,\tau)|^2}{\hbar\omega_2}. \tag{9}$$

This relation (the Manley-Rowe relation) reflects the fact that induced transitions in the two-level system are accompanied by simultaneous emission (or absorption) of two quanta $\hbar\omega_2$ and $\hbar\omega_3$.

In the following it is convenient to introduce the parameter

$$\beta=(q_{12}/r_{12}) \tag{10}$$

characterizing a relative strength of resonant coupling. Experimentally, in order to additionally increase the efficiency of the FWDFM process the generated field frequency is usually tuned in the vicinity of resonance with some intermediate atomic level (m) [that means that in Eq. (5) $|\omega_3-\omega_{m1}| \ll\omega_3$], and in most practical cases β is much larger than 1.

First we analyze the initial (linear) stage of frequency conversion at which the pump field temporal distribution is still close to its input one, i.e., $E_1(z,\tau)\approx E_1(\tau)$ and the influence of fields E_2 and E_3 on the state of the resonant transition can be neglected. According to the Bloch equations (3), this is the case as long as the condition $|E_1|^2 \gg\beta|E_2E_3|$ holds. The solution of Eqs. (8) for the generated field at this stage is

$$|E_3(z,\tau)|^2=\frac{\omega_3}{\omega_2}\,|E_2(\tau)|^2\,\frac{G_0^2}{G^2}\,sh^2(Gz). \tag{11}$$

Here the time-dependent increment $G(\tau)$ of the generated field is determined by

$$G(\tau)=\sqrt{G_0^2(\tau)-[\Delta K(\tau)/2]^2},$$

$$G_0(\tau)=\frac{2\pi N}{c}\,(\omega_2\omega_3)^{1/2}q_{12}|\sigma_{12}(\tau)|, \tag{12}$$

where $\Delta K(\tau)$ is the full nonstationary wave-number mismatch

$$\Delta K(\tau)=\Delta k+\delta_2(\tau)+\delta_3(\tau)-2\,\delta_1(\tau), \tag{13}$$

with $\delta_i(\tau)=2\pi N\omega_i c^{-1}[\sigma_{11}(\tau)\alpha_{11}^{(i)}+\sigma_{22}(\tau)\alpha_{22}^{(i)}]$. The temporal behavior of the medium response $\sigma_{ij}(\tau)$ entering Eqs. (12) and (13) is obtained by solving Bloch equations (3) with the pump field $E_1(\tau)$.

Expression (11) is similar to the one arising in the theory of parametric generation [16,17], and in the case $\Delta K\gg G_0$ it turns into the commonly used formula for intensity of the difference frequency signal. From Eqs. (11) and (12) it follows that the intensity of the difference-frequency field can be further increased by maximizing the value of the nondiagonal matrix element σ_{12} and the coupling constant q_{12} (or β) as well as by increasing the injected pulse intensity $|E_2(\tau)|^2$. However, as will be shown below, due to resonant saturation effects such a simple optimization procedure does not necessary lead to higher conversion efficiencies for the FWDFM process, and the nonlinear stage of frequency conversion has to be analyzed.

We concentrate now on a study of the nonlinear stage of FWDFM and consider characteristics of resonant frequency conversion in two cases of practical importance: in the case of relatively large frequency detunings (quasiresonant interaction), and in the case of on-resonant interaction. The fact that experimentally the parameter β is large ($\beta\gg1$) allows us, in the subsequent discussion, to assume the condition

$$\beta\,\frac{(\omega_2\omega_3)^{1/2}}{2\omega_1}\gg1, \tag{14}$$

which implies physically [see Eqs. (8)] that the two-photon process involving fields E_2 and E_3 develops on an interaction length sufficiently shorter than the characteristic length of two-photon interaction for the pump field E_1.

B. Quasiresonant interaction

Let us assume that the detuning $\Delta\Omega$ of the laser field frequency from the two-photon transition frequency considerably exceeds the spectral widths $\Delta\nu_i$ of the pulses,

$$|\Delta\Omega|\gg\Delta\nu_i, \quad i=1,\ 2,\quad \text{and}\ 3. \tag{15}$$

In this situation the laser-atom interaction can be described in terms of the ''adiabatic following'' model [19]. According to this model, the atomic response ''follows'' the instantaneous value of an incident field. Indeed, neglecting the term $\partial\sigma_{12}/\partial\tau$ in comparison to the term $\Delta\Omega\sigma_{12}$ in the Bloch equations (3) and taking into account the ultrashort-pulse condition (1), the solution of Eq. (3a) for the medium excitation σ_{12} can be written as

$$\sigma_{12}=\frac{r_{12}}{4\hbar}\,\Delta\Omega^{-1}n(E_\Sigma^*)^2, \tag{16}$$

where the effective resonant field $E_\Sigma^2=(E_1^2+\beta E_2E_3e^{i\Delta kz})$ has been introduced.

On the other hand, on the ultrafast time scale (2) the Bloch equations (3) satisfy the probability conservation law [10]

$$4|\sigma_{12}|^2+n^2=1. \tag{17}$$

By combining Eqs. (16) and (17), we obtain the following solution for the material variables:

$$\sigma_2=\frac{r_{12}}{4\hbar}\,\frac{(E_\Sigma^2)^*}{\Delta\Omega}\Bigg/\left(I+\frac{r_{12}^2}{4\hbar^2}\,\frac{|E_\Sigma^2|^2}{\Delta\Omega^2}\right)^{1/2}, \tag{18}$$

$$n=-1\Big/\left(1+\frac{r_{12}^2}{4\hbar^2}\frac{|E_\Sigma^2|^2}{\Delta\Omega^2}\right). \tag{19}$$

We suppose below that the atomic transition is far from saturation [that means that in Eqs. (18) and (19) $r_{12}|E_\Sigma^2|/(4\hbar\Delta\Omega)\ll 1$]. In accordance with condition (14), to a good approximation we can restrict our subsequent analysis to a study of the evolution of the fields E_2 and E_3, with the pump field E_1 close to its input value $E_1(\tau)$. By inserting solution (18) for the medium response into Eqs. (8b) and (8c), and assuming ideal phase synchronizm conditions ($\Delta K=0$), we derive the equations

$$\frac{\partial E_2}{\partial\zeta}=i\omega_2(E_1^2E_3^*+\beta E_2|E_3|^2), \tag{20a}$$

$$\frac{\partial E_3}{\partial\zeta}=i\omega_3(E_1^2E_2^*+\beta E_3|E_2|^2), \tag{20b}$$

where the variable $\zeta=z(\pi Nr_{12}^2/4c\hbar\Delta\Omega)$ proportional to the propagation length z has been introduced. Assuming the pump field complex amplitude to be real ($E_1E_1=|E_1|^2$) and using the conservation law (9) for the photon number difference, Equations (20) can be reduced to only one equation for the generated field intensity:

$$\frac{\partial|E_3|^2}{\partial\zeta}=2\omega_3|E_1(0)|^4\sin\left[\beta^2\int_0^\zeta[2\omega_2|E_3|^2+\omega_3|E_2(0)|^2]d'_\zeta\right]. \tag{21}$$

Since E_3 and E_2 depend on τ only parametrically (through the boundary conditions), we have omitted the τ dependence in Eq. (21), and denoted for brevity the input values of the pump and injected field at $\zeta=0$ by $E_1(0)$ and $E_2(0)$, respectively. It can be seen that Eq. (21) reduces to the pendulum equation and describes spatial oscillations of the generated field intensity along the propagation distance ζ. Solution of Eq. (21) has the form

$$|E_3(\zeta)|^2=\frac{1}{2}\frac{\omega_3}{\omega_2}|E_2(0)|^2[\mathrm{dn}^{-1}(a\zeta/b,b)-1], \tag{22}$$

where $\mathrm{dn}(u,k)$ is the elliptic Jacobi function, $a^2=4\beta^2\omega_2\omega_3|E_1(0)|^4$, and $b^2=\{1-|E_2(0)|^2/[|E_2(0)|^2+2\omega_2\omega_3^{-1}|E_3|_{\max}^2]^2\}$ with $|E_3|_{\max}^2$ denoting the maximum value of the generated field intensity in the spatially periodical process

$$|E_3|_{\max}^2=\left(\frac{1}{4}\frac{\omega_3^2}{\omega_2^2}|E_2(0)|^4+\frac{4}{\beta^2}\frac{\omega_3}{\omega_2}|E_1(0)|^4\right)^{1/2}-\frac{1}{2}\frac{\omega_3}{\omega_2}|E_2(0)|^2. \tag{23}$$

The maximum value (23) is achieved at the interaction lengths $\zeta_m=a^{-1}bK(b)(2m+1)$, where $m=0,1,2,\ldots$, and $K(k)$ is the complete elliptic Legendre integral. According to formula (23), with an increase of the pump field $E_1(0)$ the value of $|E_3|_{\max}$ also increases. This seems to be quite consistent with the above assumption of a weakly saturated resonance transition. But in contrast to the dependence predicted by formula (11) of the initial stage of FWDFM, $|E_3|_{\max}$ shows a monotonic decrease with increasing $E_2(0)$ and β. The optimum value of $|E_3|_{\max}$ corresponds to the formal limit $E_2(0)\to 0$ in Eq. (23), and is given by

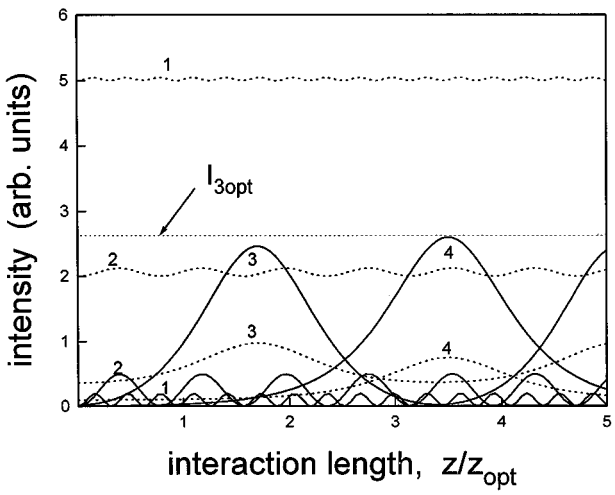

FIG. 2. Nonlinear stage of near-resonant difference-frequency generation under the condition of collinear phase matching. Intensities of the injected v (dotted line) and generated (solid line) fields as functions of the interaction length z for different relative values of the injected field input intensity [1, $I_2(0)/I_1(0)=0.25$; 2, $I_2(0)/I_1(0)=0.1$; 3, $I_2(0)/I_1(0)=0.02$, 4, $I_2(0)/I_1(0)=0.005$] and with $\beta=20$.

$$|E_3|_{\mathrm{opt}}^2=\frac{2}{\beta}\left(\frac{\omega_3}{\omega_2}\right)^{1/2}|E_1(0)|^2. \tag{24}$$

In this limiting case, solution (22) for $E_3(z)$ becomes an aperiodical one,

$$|E_3(z)|^2=|E_3|_{\mathrm{opt}}^2\frac{1}{\cosh(z/z_{\mathrm{opt}})}. \tag{25}$$

The solution trends to zero in the limits $z\to\pm\infty$. It describes a buildup of the generated field E_3 from spontaneous noise due to the parametrical-oscillation process, and a subsequent decrease of the field due to the reverse process of a return of the generated field energy back to the pump field. The process develops on the characteristic spatial scale

$$z_{\mathrm{opt}}=\frac{2\omega_1}{(\omega_2\omega_3)^{1/2}}\frac{L_1}{\beta}, \tag{26}$$

where $L_1=c\hbar\Delta\Omega/(2\pi N\omega_1r_{12}^2|E_1(0)|^2)$ is the two-photon interaction length for the pump field. If the input intensity of E_2 is not too high so that the condition $\beta|E_2(0)|^2\ll 4(\omega_2/\omega_3)^{1/2}|E_1(0)|^2$ is fulfilled, the maximum value (23) is close to the optimum value (24). The propagation length z_0 corresponding to the first maximum of E_3 is then in the order of magnitude of the length (26).

Figure 2 shows the intensities of the generated and injected fields as a function of the active region length z calculated with formula (22) for different input values of the injected field intensity. As can be seen, higher input values

of the injected field result in higher values of the generated field only at the linear stage of frequency conversion ($z/z_{opt} \ll 1$). But at longer interaction lengths ($z \geqslant z_{opt}$), where saturation takes place, the higher the input value of the injected field, the lower the maximum achievable efficiency. From the above analysis it follows that an optimum regime of FWDFM is realized when the injected field strength $E_2(0)$ is rather weak in comparison to $E_1(0)$. In this regime, the linear stage of the process is characterized by an exponential increase of both E_3 and E_2 that leads [according to the Manley-Rowe relation (9)] to a formation of fields with nearly equal number of photons,

$$\frac{|E_3(z)|^2}{\hbar\omega_3} \approx \frac{|E_2(z)|^2}{\hbar\omega_2} \gg \frac{|E_2(0)|^2}{\hbar\omega_2}. \tag{27}$$

At the nonlinear stage, the field intensities exhibit spatial oscillations with the oscillation amplitudes close to $|E_3|^2_{opt}$ and $(\omega_3/\omega_2)|E_3|^2_{opt}$, respectively.

The observed features of the nonlinear regime of FWDFM can be explained by counteraction between two-photon absorption of the pump field quanta and two-photon emission of the generated and injected field quanta. When the term $q_{12}|E_2E_3|$ in the material equations (3) becomes comparable to the term $r_{12}|E_1|^2$, a compensation of the resonant contribution of the two processes occurs, leading to a reduction of the value of the medium excitation σ_{12} and thereby to a saturation of conversion. Due to concurrent accumulation of the nonlinear phase shift between the waves over the propagation length, the FWDFM process has the form of spatial beats of the field amplitudes. It should be noted that the nature of this saturation is quite different from the mechanism of saturation of a two-level system in a strong field [10]. In the latter case the saturation of the resonant polarization results from saturation of atomic populations, whereas in the discussed situation σ_{12} is saturated even when field-induced change of populations is relative small.

Using Eq. (24), we can now estimate the maximum conversion efficiency for the FWDFM process,

$$\eta = |E_3|^2_{opt}/|E_1(0)|^2 = \frac{2}{\beta}\left(\frac{\omega_3}{\omega_2}\right)^{1/2}. \tag{28}$$

From formula (28) it follows that an additional quasiresonant enhancement of the matrix element q_{12} (or increase of β) generally leads to a decrease of the optimum conversion efficiency if β is sufficiently large [see condition (14)]. On the other hand, in the limit $\beta \ll 1$, the discussed saturation effect is negligible, and FWDFM is described by formulas (11)–(13) of the linear stage which predict a monotonic decrease of η when β trends to zero [$\eta(\beta) \propto \beta^2$, assuming $\Delta K = 0$]. This suggests that $\eta(\beta)$ should have a maximum in the region $\beta \sim 1$. The corresponding value of the coupling parameter can be estimated to be about $\beta^* \sim 4\omega_1/(\omega_2\omega_3)^{1/2}$ and in the optimum regime conversion efficiencies up to several tens of percent can be expected. Experimentally, the values of β lie typically in the range 10^1–10^2 where, according to Eq. (28), maximum achievable efficiencies are of the order of $\eta \sim (10^{-1}$–$10^{-2})$ that is close to the experimentally observed values [6–8].

C. Resonant interaction

We now turn to a discussion of the FWDFG process in the case of resonant interaction, i.e., when the condition

$$|\Delta\Omega| < \Delta\nu_i, \quad i = 1, 2, \quad \text{and } 3 \tag{29}$$

is fulfilled. Together with relation (2), condition (29) means that the regime of coherent laser-atom interaction takes place. As will be shown, in this interaction regime resonant propagation phenomena such as self-induced transparency and the effects of nonlinear amplitude and phase modulation play a dominating role in the frequency conversion process. The interesting feature of coherent FWDFM is that the process can be accompanied by a nonlinear pulse compression and generation of ''two-color'' pulses at the difference and the injection frequency with durations sufficiently shorter than the input injection pulse duration. Such pulses represent 2π pulses of two-photon self-induced transparency, and therefore propagate through the two-photon absorber without attenuation.

The initial stage of the FWDFM process [at which the pump field is still close to its input value $E_1(\tau)$] is described by the general expression (11), where the temporal dynamics of the two-photon transition is determined by solving Bloch Eqs. (3) for σ_{ij} with the pump field $E_1(\tau)$. At exact resonance $\Delta\omega = 0$, the solution has a form

$$\sigma_{12}(\tau) = \frac{\gamma(\cos\Psi_1 - 1)}{2(1+\gamma^2)} + i\,\frac{\sin\Psi_1}{2(1+\gamma^2)^{1/2}},$$

$$n(\tau) = \frac{(1-\cos\Psi_1)}{(1+\gamma^2)} - 1, \tag{30a}$$

where the pump field is assumed to be real, i.e., $E_1E_1 = |E_1|^2$, and the rotation angle

$$\Psi_1(\tau) = \frac{r_{12}}{2\hbar}(1+\gamma^2)^{1/2}\int_{-\infty}^{\tau}|E_1(\tau')|^2 d\tau' \tag{30b}$$

proportional to the pump field instantaneous energy is introduced; the parameter $\gamma = (\alpha_{22}^{(1)} - \alpha_{11}^{(1)})/2$ accounts for the contribution of the dynamical Stark effect into the rotation angle. According to Eq. (30a), the population difference n and the excitation σ_{12} are oscillating functions of Ψ_1 (two-photon Rabi oscillations). Therefore an increase of the pump pulse energy above the value which provides a maximum for the increment G of the generated field is not needed. Furthermore, since the relaxation times are assumed to be long compared to the pulse durations, a frequency conversion regime in which the injected pulse propagates with a delay $\Delta\tau < T_2$ with respect to the pump pulse, and which interacts with the coherently excited medium, should be possible.

Now we consider the nonlinear stage of the FWDFM process when the influence of the fields E_2 and E_3 on the state of the resonant transition has to be taken into account. We will focus our subsequent analysis on the regime of delayed pulse propagation. This regime is of interest because, for sufficiently large temporal delays $\tau_{pl} < \Delta\tau < T_2'$, the direct influence of the pump field on the difference-frequency signal can be eliminated. Let the injected pulse propagate with a time delay $\Delta\tau \ll T_2'$. Neglecting for simplicity the difference

in the values of level polarizabilities and assuming $\Delta k=0$, we obtain the following solution of Bloch Eqs. (3):

$$\sigma_{12}(\tau)=\frac{i}{2}\sin\Psi_{\Sigma},\quad n(\tau)=-\cos\Psi_{\Sigma},\tag{31}$$

where $\Psi_{\Sigma}=\theta_1+(q_{12}/2\hbar)\int_{-\infty}^{\tau}E_2E_3d\tau'$ and $\theta_1=(r_{12}/2\hbar)\int_{-\infty}^{\infty}|E_1|^2d\tau$ is the full rotation angle produced by the pump pulse. It can be shown that the sign of the product (E_2E_3) is determined by the sign of the imaginary part of $\sigma_{12}(\tau)$ at the medium input $z=0$. Taking this fact into account and combining Eqs. (8) with Eqs. (31), one can construct the equation for the spatial evolution of the full rotation angle $\theta_2(z)=(q_{12}/2\hbar)\int_{-\infty}^{\infty}E_2E_3d\tau$ produced by the ''two-color'' E_2E_3 pulse,

$$\frac{d\theta_2}{dz}=\Phi(\theta_1,\theta_2)=2\beta\alpha_1(\mathrm{sgn}\,[\sin\theta_1(0)])[\cos\theta_1-\cos(\theta_1+\theta_2)],\tag{32a}$$

where $\alpha_1=2\pi\omega Nr_{12}/c$ is the two-photon absorption coefficient for the pump field and the function sgn$[x]$ takes a value of -1 if $x<0$ and $+1$ if $x>0$. The evolution of the pump pulse rotation angle $\theta_1(z)$ with the propagation distance z obeys the ''energy theorem'' [11]

$$\frac{d\theta_1}{dz}=-2\alpha_1(1-\cos\theta_1).\tag{32b}$$

Because of the assumption $\beta\ll1$, the pump pulse rotation angle θ_1 changes rather slowly in comparison to θ_2. Therefore Eq. (32a) describes the evolution of a small initial angle $\theta_2\ll\theta_1$ toward the stable value θ_2^*, which is defined by the conditions $\Phi(\theta_1,\theta_2^*)=0$ and $d\Phi(\theta_1,\theta_2^*)/d\theta_2<0$, and depends parametrically on the actual value of the pump pulse angle θ_1. If, for example, the value of the pump pulse angle θ_1 lies in the region $0<\theta_1<\pi$, then a small initial angle $\theta_2\ll\theta_1$ evolves toward the stable value $\theta_2^*=-2\theta_1$. In the case $\pi<\theta_1<2\pi$, a small initial angle tends to the stable value $\theta_2^*=2(2\pi-\theta_1)$. The dynamics of the ''two-color'' pulse reflects, in fact, the tendency to propagate without energy loss: the leading edge of the pulse is amplified by the excited medium; its trailing edge experiences nonlinear attenuation. Computer simulations of the dynamic of the interacting pulses show that, concurrently with the angle stabilization, a considerable nonlinear compression of the two-color pulse duration is observed (see Fig. 3). At propagation lengths at which two-photon absorption of the pump field becomes considerable, the second stage of frequency conversion develops. Depending on the pump pulse initial angle $\theta_1(0)$, the following two scenaria are realized. If $0<\theta_1(0)<\pi$ and $\theta_2^*=-2\theta_1$, the process of pump pulse two-photon absorption described by Eq. (32b) leads to an adiabatically slow absorption of the two-color pulse ($\theta_2^*\to0$). In the second case, when $\pi<\theta_1(0)<2\pi$ and $\theta_2^*\approx2(2\pi-\theta_1)$, the pump pulse angle θ_1 decreases whereas the two-color pulse angle (and energy) continue to increase. When the pump pulse angle approaches the value $\theta_1\approx\pi$ the two-color pulse becomes a 2π pulse of self-induced transparency. At longer propagation lengths the pump pulse energy is absorbed in the resonant medium, and the two-color pulse propagates through the medium without attenuation (see Fig. 3). It can be seen that intensities of fields E_2 and E_3 are substantially higher than that of the input field $E_2(0)$. According to Eq. (9), the field amplitudes in the compressed pulse are nearly proportional. Using the fact that generation of a two-color 2π pulse requires pump pulses with the rotation angle in the region $\pi<\theta_1<2\pi$, we can estimate the maximum conversion efficiency for the process. Taking $\theta_1=\pi$ and $\theta_2^*=2\pi$, we obtain the value

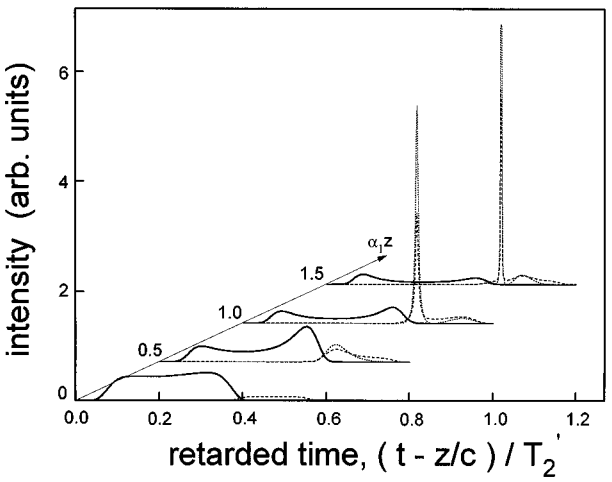

FIG. 3. Computer simulation of the dynamics of coherent resonant FWDFG in the regime of delayed pulse propagation. The pump pulse (solid), the injected pulse (dashed), and the generated vuv pulse (dotted) intensity temporal distribution as a function of propagation length z. The length z is expressed in units of the inverse of the pump pulse two-photon absorption index α_1, the retarded time is normalized by the polarization relaxation time T_2'. The pump pulse input area is $\theta_1=1.5\pi$, and the relations between frequencies and input energies of the pump and the injected pulse are assumed to be $\omega_1/\omega_2=1.5$, and $W_1(0)/W_2(0)=50$, respectively.

$$\eta=\int_{-\infty}^{\infty}|E_3|_{2\pi}^2d\tau\Big/\int_{-\infty}^{\infty}|E_1(0,\tau)|^2d\tau=\frac{2}{\beta}\left(\frac{\omega_3}{\omega_2}\right)^{1/2}.\tag{33}$$

Although the maximum efficiency estimation is seen to coincide with the one for the near-resonant process (28), the mechanism of saturation here is different. Unlikely the quasiresonant case, in the discussed coherent regime of FWDFM the injected pulse is substantially delayed with respect to the pump pulse, and no direct interference of the two resonant processes occurs. But, because of the coherent propagation effects, the vuv pulse energy gain is limited to a formation of the two-color pulse with the stable value of rotation angle and energy. Again, estimation (33) shows that higher conversion efficiencies can be obtained in the resonant media when the parameter β is not very large compared to one. On the base of our computer calculations it has been found that a maximum efficiency (up to 20–30 %) is realized if the characteristic generation length ($L_g\sim G_0^{-1}$) of the fields E_2 and E_3 is only 2–3 times shorter than the pump pulse two-photon absorption length ($L_1\sim\alpha_1^{-1}$). This means that the optimum value of the coupling parameter is about $\beta^*\sim2\omega_1/(\omega_2\omega_3)^{1/2}$. In Fig. 3 we show the results of computer

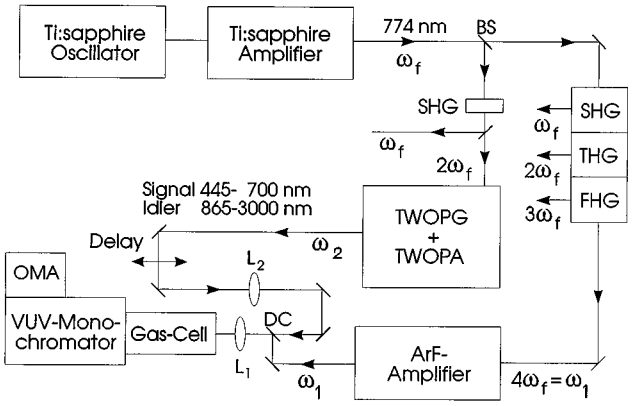

FIG. 4. Block diagram of the experimental setup: BS, beam splitter; DC, dichroic mirror; SHG, second-harmonic generation; THG, third-harmonic generation; FHG, fourth-harmonic generation; TWOPG, traveling-wave optical parametric generator; TWOPA, traveling-wave optical parametric amplifier; OMA, optical multichannel analyzer.

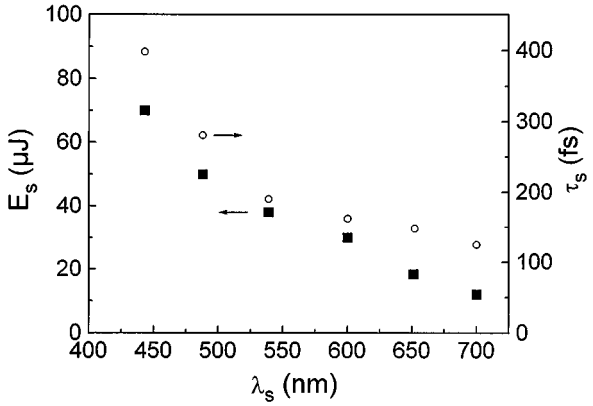

FIG. 5. Energy E_s (■) and pulse duration τ_s (○) of the signal pulses of the parametric system as a function of its wavelength λ_s.

modeling of coherent resonant FWDFM in noble gases assuming the values of the two-photon matrix elements $r_{12} \sim 10^{-24}$ cm^3 and $\beta = (q_{12}/r_{12}) = 5$. The calculation shows that a conversion efficiency of about 20% with an additional temporal self-compression of the vuv pulse up to a factor 10 can be achieved at propagation lengths of only several cm for resonant atom concentrations $N \sim 10^{18}$ cm^{-3}.

II. DIFFERENCE-FREQUENCY MIXING EXPERIMENTS

The experimental setup is shown in Fig. 4. We employed a homemade Ti:sapphire oscillator-amplifier system providing 8-mJ, 80-fs (0.1-TW) output (fundamental) pulses at a wavelength tunable around 774 nm with 10-Hz repetition rate. Temporal stretching of the 50-fs, 4-nJ output pulses of the oscillator (75-MHz repetition rate) to 100 ps is accomplished in a grating stretcher (1200 lines/mm) using reflective optics. First these pulses are amplified to pulse energies of about 1.3 mJ in a regenerative amplifier (arranged in a three mirror configuration similar to Ref. [20]) which is pumped by 5 mJ of the 120-mJ, 7-ns output of a Q-switched frequency-doubled Nd:YAG (neodymium-doped:yttrium aluminum garnet) laser. Further amplification up to 18 mJ is established in a three-pass power amplifier pumped with the main part of the Nd:YAG output. Finally the positively chirped amplified pulses are compressed in a conventional double-pass grating compressor.

Quadrupling one part (2 mJ) of the intense Ti:sapphire fundamental output in a cascaded second-order sum-frequency mixing scheme $[\omega \rightarrow 2\omega(\omega+\omega) \rightarrow 3\omega(2\omega+\omega) \rightarrow 4\omega(3\omega+\omega)]$ employing three β barium borate (BBO) crystals [21] provides nearly 10-μJ, 150-fs seed pulses at 193 nm. Subsequent amplification of these pulses in a commercial ArF gain modul (EMG 150 MSC) in a double-pass configuration resulted in $\approx$1.5-mJ, 250-fs pulses [22] which serve as pump pulses (ω_1) in the FWDFM scheme.

In addition to this strong pump laser field at 193-nm efficient FWDFM requires the injection of powerful femtosecond pulses [injection pulses (ω_2)] synchronized to the ArF output pulses. Therefore a second part of the fundamental radiation is frequency doubled in a 0.5-mm-long BBO crystal resulting in 0.5-mJ pulses at 387 nm which were used to pump a traveling-wave optical parametric generator (TWOPG) system consisting of an optical parametric generator (4-mm BBO, Typ II, $\theta = 37°$) and a traveling-wave optical parametric amplifier (TWOPA) (6-mm BBO, Typ I $\theta = 28°$) arranged in a configuration similar to Ref. [23]. Seeding the TWOPG with femtosecond continuum radiation produced with some 10 μJ of the fundamental radiation in a 4-mm-thick plate of fused silica stabilized and increased the output performance of the parametric system [23]. Varying the phase-matching angles of the crystals, the wavelength of the signal could be tuned from 445 nm to about 700 nm (Fig. 5), corresponding to an idler tuning range of 865–3000 nm.

As depicted in Fig. 5, the energy of the generated signal pulse increases with decreasing wavelength, since the reduction of the group velocity mismatch between signal and pump pulse permits a higher interaction length in the TWOPA. At the same time this increased interaction length leads to saturation of the amplification due to pump pulse depletion, which gives rise to a temporal broadening of the signal pulse. From earlier experiments we know that the pulse duration of the idler radiation is somewhat shorter than that of the signal radiation, since the idler is generated only during the amplification of the signal within the field of the 387-nm pump pulse [24]. Below a signal wavelength of 445 nm, we observed a sharp drop of the TWOPA performance which can be attributed to suppression of the parametric process due to strong absorption of the idler radiation in the nonlinear crystal above a wavelength of 3 μm.

Finally the pump pulse (ω_1) and the tunable injection pulse (ω_2) are combined on a dichroic mirror and focused with a thin MgF_2 lens (L_1, $f = 60$ cm) into a gas cell ($L = 55$ cm). The spot size of the pump radiation at the focus position was measured by a sharp edge method to be 140×180 μm^2 corresponding to an area of 2×10^{-4} cm^2. With 0.5 mJ of input energy behind the entrance window (0.5-cm MgF_2), the focused intensity in the cell is nearly 10 TW/cm^2.

The temporal overlap between the pump and the injection pulses is accomplished through an optical delay line and by means of lenses L_2 with different focal lengths (2-mm fused silica, $f = 100-400$ cm) we tried to match the focus position

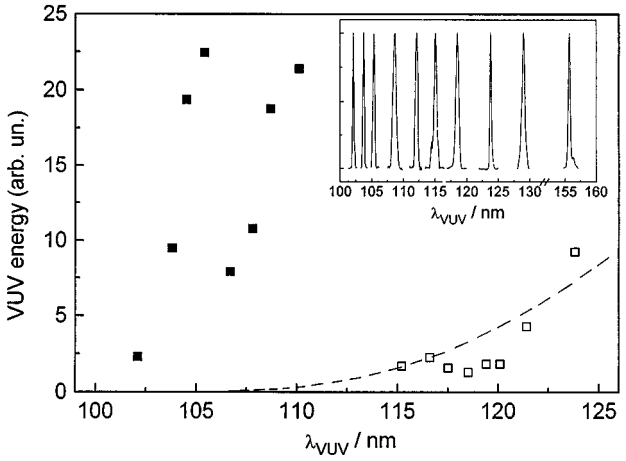

FIG. 6. Relative vuv energy values for the FWDFM (open squares, argon, filled squares: krypton) as a function of the generated vuv wavelengths. Inset: selected number of spectra of the generated femtosecond tunable vuv radiation (102–124 nm) and spectra of the radiation at 129 and 155 nm generated by mixing ω_1 with fixed frequencies ($2\omega_f$ and $3\omega_f$). The employed OMA system had a spectral resolution of 0.06 nm/channel. Note the break on the X axis to show the whole spectral range while keeping a reliable resolution of the spectra. Dashed line, the wavelength dependence of the efficiency of the vuv generation in Ar predicted by formula (35).

and spot size of the injection radiation with that of the pump radiation.

The generated vuv radiation was spectrally separated from the pump and the injection radiation by a 0.2-m vuv monochromator (McPherson Model 234/302) and detected with an uv-enhanced optical-multichannel-analyzer system. In order to avoid strong absorption, especially for the shortest vuv wavelengths (below the LiF cutoff), we removed the output window of the gas cell, thus filling the monochromator with the nonlinear medium, too.

III. DIFFERENCE-FREQUENCY GENERATION RESULTS AND THEIR DISCUSSION

A selection of the spectra of the generated vuv radiation is shown as an inset in Fig. 6. It should be noted that the radiation in the spectral range from 112 to 124 nm was generated by mixing the pump radiation with the tunable signal radiation in argon, whereas the radiation in the range below 110 nm results from mixing with the idler in krypton. The shortest generated vuv wavelength was 102 nm, because the transmission of the optics employed in the delay path for the idler radiation strongly decreases for wavelengths above 2 μm (fused silica lenses and mirror protection coatings).

Due to the lack of an appropriate detector head which would allow the absolute energy measurement of the generated vuv pulses in the vacuum, we were not able to measure absolute values for the vuv output energy and the optical conversion efficiency. To have a relative measure for the generated vuv energy, a constant width of the entrance slit of the monochromator was used. In addition to this, care was taken to reach the maximum vuv signal by adjusting lens $L1$ and optimizing the temporal and spatial overlap of the pump and the injection pulse. Figure 6 shows the relative values of the vuv pulse energy for the FWDFM as a function of the vuv wavelength. It is interesting that in argon the conversion efficiency shows a monotonic decrease for shorter wavelengths λ_3 in the range 124–112 nm, where the generated frequency comes close to resonance with the intermediate ($4s$) atomic level. This behavior can be attributed in part to a decrease in signal output energy of the TWOPG (see Fig. 5) and to an incomplete temporal overlap of the pump and the injected pulses. In addition, in this tuning range the frequency of the radiation generated by the FWDFM lies below the first argon resonance line (106.6 nm), and in a collinear incidence of pump and injected radiation this process has a negative wave-vector mismatch, $\Delta k = 2k_1 - k_2 - k_3$, and phase matching should be possible applying a noncollinear interaction. Taking Sellmeier formulas given in [25] (and Refs. [11] and [12] therein) the angles which are required for phase matching in Ar are calculated to increase in the range 1.6°–4° when λ_3 decreases in the tuning region 124–112 nm.

Owing to the finite aperture (2 cm) of lens $L1$ and the entrance window of the glass cell, the largest angle between the pump and the injected radiation we were able to realize was nearly 0.5°, and thus the increasing wave-number mismatch could affect the FWDFM process.

On the other hand, when the frequency of the generated field comes close to a resonance with the intermediate level ($4s$), a quasiresonant enhancement of the two-photon matrix element q_{12} associated with emission of $h\omega_2$ and $h\omega_3$ photons also takes place. Assuming that the near-resonant value of q_{12} is mainly determined by the contribution of the intermediate level, expression (5) for q_{12} can be rewritten in the form

$$q_{12}(\lambda_3) = \frac{\mu_{1R}\mu_{R2}}{2\pi\hbar c} \frac{\lambda_3\lambda_R}{(\lambda_3 - \lambda_R)}, \tag{34}$$

where μ_{1R} and μ_{2R} are the dipole matrix elements of the transitions between the lower (1) or upper (2) ''working'' level and the intermediate atomic state, and λ_R is the wavelength of the resonant line (106.6 nm). From formulas (34) and (12) it follows that, in the vicinity of λ_R, the linear increment G_0 of the generated field sharply increases, and thus the observed decrease of frequency conversion efficiency cannot be explained solely by the wave-number mismatch.

We can explain the experimentally observed dependence in Ar on the base of the analysis of nonlinear stage of FWDFM (Sec. I). In Ar the two-photon energy of the pump field is detuned 690 cm^{-1} away from the resonant with the upper $3p^5 4p(1/2)_2$ level, and the regime of quasiresonant interaction (15) is realized [see the relevant scheme in Fig. 1(a)]. Let us estimate the characteristic length (or the period of spatial oscillations) at which the FWDFM process is saturated due to the interference of contributions of the two resonant processes into the medium nonlinear polarization. Using formulas (22) and (23) with the pump ($\lambda_1 = 193$ nm) and injected ($\lambda_2 \sim 700$ nm) field intensities of $I_1(0) = 10$ TW/cm^2 and $I_2(0) = 1$ TW/cm^2, respectively, and estimating the parameter β from [26] by ≈ 20, we find that the corresponding length is of the order of 10^{-2} cm and is thus substantially shorter than the length of the interaction region (~ 1 cm). Since within the interaction region the generated

field exhibits fast spatial modulations, the efficiency of the FWDFM process can be estimated by averaging the generated field intensity (22) over the spatial period. For large β this yields $\langle|E_3|^2\rangle \approx 0.5|E_3|^2_{\max}$, where $|E_3|^2_{\max}$ is given by Eq. (23). Approximating β by the near-resonant expression (34) and calculating $\langle|E_3|^2\rangle$ with the above values of the pump and the injected field intensity, we obtain the following formula for the conversion efficiency frequency dependence:

$$\eta(\lambda_3) = [\sqrt{A^2 + B^2(\lambda_3 - \lambda_R)^2} - A], \tag{35}$$

with $A = 0.125$ and $B = 0.05\ \mathrm{nm}^{-1}$. The dependence is depicted in Fig. 6 together with experimental data. The calculated frequency dependence is seen to be in a qualitative agreement with the observed behavior, and this suggests that the discussed resonant saturation effects can play an important role in the FWDFM process.

In krypton the interpretation of the vuv energy dependence on the wavelength is more difficult. Unlike the case of Ar, in Kr the pump pulse carrier frequency was in a two-photon resonance with the $4p^5 6p(3/2)_2$ state within the pulse spectral bandwidth [see the relevant scheme in Fig. 1(b)]. Hence the regime of resonant interaction took place. The spectroscopic data for Kr and our experimental observations indicate that at the used pump pulse parameters ($\tau_{\mathrm{pl}} \sim 250$ fs, $I_1 \sim 10\ \mathrm{TW/cm^2}$), in addition to excitation of the upper resonant level, a number of neighboring upper atomic levels were excited. In order to describe this special situation one should use an essentially more complicated (multilevel) model of radiation-atom interaction. This is beyond the scope of the present analysis. In addition, in krypton the generated vuv radiation (110–102 nm) is above the first (123.6 nm) and the second (116.5 nm) resonance lines, and below two other resonance lines at 103 and 100.4 nm. Because of this no general trend of the conversion efficiency as a function of λ_{vuv} could be observed, but it seems to be higher than in argon. Calculations for trippling in krypton [25] show that the wave-vector mismatch is strongly wavelength dependent in this spectral region, and therefore a rapid variation of the angle necessary for phase matching should be expected. This could explain the rather irregular behavior of the relative conversion efficiency.

In addition to the tunable parametrically generated radiation, the synchronized femtosecond pulses at fixed wavelengths 774, 387, and 258 nm corresponding to the fundamental (ω_f), second ($2\omega_f$) and third harmonic ($3\omega_f$) internally generated in our cascaded sum-frequency mixing scheme (see Fig. 4) were used as injection pulses to produce vuv radiation at 110, 129, and 155 nm. The difference between the quasiresonant and resonant FWDFM processes can be seen from Fig. 7, where the generated vuv signal at $\lambda_3 = 155$ nm is shown in the dependence on the temporal delay between the pump and injection pulses. As can be seen for the case of nonresonant interaction in argon, a substantial vuv signal is produced only during a temporal overlap of the pump and the injection radiation. In contrast to this, in the case of krypton a significant difference frequency signal was detected even for delays of 100 ps. From this behavior we conclude that in the resonance case the generation of femtosecond vuv pulses at ω_3 is only possible when short femtosecond pulses at ω_2 are injected. At the same time, the obtained results represent in fact an indication of the coherent character of the femtosecond-pulse resonant FWDFM process.

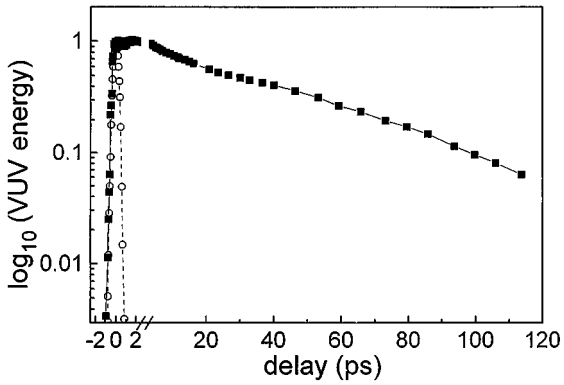

FIG. 7. Normalized FWDFM signal ($\omega_{155} = 2\omega_{193} - \omega_{258}$) depending on the temporal delay between pump and injected pulse for argon (○, $p = 80$ mbar) and krypton (■, $p = 20$ mbar). The marks represent measurement points while the lines are included to guide the eyes of the reader. Note the break on the X axis to show the first part of the curve (-2 to 2 ps) with a higher resolution.

IV. FEMTOSECOND-PULSE FWDFM AS A SPECTROSCOPIC TOOL FOR STUDYING ATOMS IN STRONG LASER FIELDS

The technique of two-photon resonant four-wave mixing with intense pump pulses and relatively weak injected (probe) pulses represents a very powerful tool for spectroscopic studies of ultrafast processes in solids, liquids, and gases [14,15]. However, so far the technique has mainly been used for studying the temporal evolution of a quantum system after it is excited by an intense pump pulse, and to our knowledge has never been employed to study dynamics of radiation-matter interaction itself. Previous experiments on two-photon resonant interaction of ultrashort pulses with atomic vapors [27,18] reported a pulse breakup into subpulses and an increase of transparency of the optically thick medium (two-photon self-induced transparency [11]). These effects, however, give only indirect information about the state of the medium. Recently, we demonstrated experimentally that the use of probe pulses significantly shorter than the pump pulses opens up the possibility of directly investigating the coherent dynamics of quantum transitions in a strong laser field. This experimental technique enabled us to observe two-photon Rabi oscillations in atomic Kr, and can be extremely important for the optimization of resonant four-wave mixing experiments.

The pump and injected pulses in these experiments were derived from the same fundamental output pulses of a 0.1-TW Ti sapphire laser by nonresonant sequential frequency mixing process (see Sec. II), which assured that they are perfectly synchronized on the femtosecond time scale. Tripling one part of the fundamental pulse by a cascaded sum-frequency mixing scheme provided 150-fs pulses at ω_2 ($\lambda_2 = 258$ nm). For quadrupling we employed a 0.5-mm-

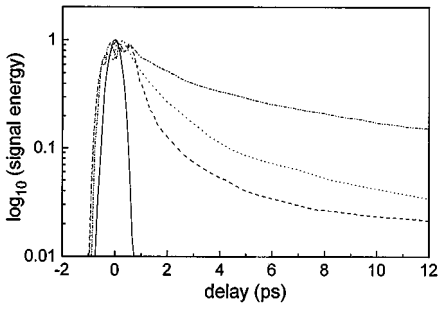

FIG. 8. Measured pulse energy of the difference-frequency signal at ω_3 as a function of the delay between the pump (ω_1) and the injected (ω_2) pulses in Ar (solid line, $p=80$ mbar) and Kr (dashed line, $p=500$ mbar; dotted line, $p=120$ mbar; dashed–double-dotted line, $p=25$ mbar) with $W_1=450$ μJ and $\tau_{\rm pl}=550$ fs.

long BBO crystal in the third mixing stage ($3\omega_f+\omega_f\rightarrow 4\omega_f$) which had an acceptance bandwidth smaller than the spectral width of the incident radiation. Therefore only a part of the incident spectrum can contribute effectively to the frequency mixing process, thus leading to spectrally narrowed and temporally lengthened pulses at 193 nm. Using a cross-correlation technique [19] the temporal width (full width at half maximum) of the amplified 193-nm pulses was measured to be 550 fs. Pumping with these pulses and probing with the three-times-shorter injection pulses made it possible to resolve Rabi oscillations induced by the strong two-photon interaction of the pump pulses with the atomic medium. By varying the angle of the BBO crystal the center frequency of our 193-nm seed pulses was tunable within the bandwidth of the ArF gain profile. Thus we were able to excite the $4p^6\ {}^1S_0\rightarrow 6p(5/2)_2$ two-photon transition in krypton resonantly. The exact resonance was verified by generating a maximum yield of the 123.6-nm fluorescence line of Kr and measuring the wavelength of the pump pulses. A relative measure of the energy at the difference frequency was determined by integration over the spectrum which was recorded with a charge-coupled device detector after being properly filtered through a 0.2-m vuv monochromator.

Using Ar and Kr as nonlinear media, two qualitatively different pictures of the medium response behavior have been observed. In Ar, where the frequency detuning from the nearest two-photon resonance was large (≈ 690 cm^{-1}) compared to the pump pulse spectral width $\Delta\nu_1$ (~ 55 cm^{-1}), a noticeable difference-frequency signal was observed only when the pump and the injected pulse overlapped each other in time. The corresponding dependence of the signal on the delay time represented a shape directly related to that of the pump pulse intensity (see Fig. 8, solid line).

In contrast, for two-photon excitation of Kr the dependence of the signal on the delay time shows a slow decay (Fig. 8), and a signal could be detected for delays as long as 20–30 ps. With an increase of the gas pressure the decay time decreased monotonically. We also observed an oscillating substructure in the region where the pump and injected pulses had a substantial temporal overlap. The substructure appeared only at pump pulse energies exceeding a critical value of 70–80 μJ, corresponding to a fluence of 0.35–0.4 J/cm^2 (2×10^{-4} cm^2 focal spot size). The characteristic time scale of these oscillations became shorter the

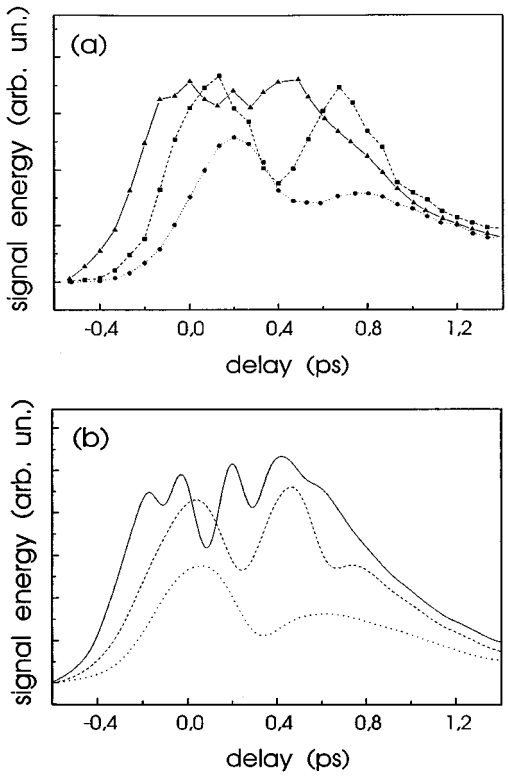

FIG. 9. (a) Measured pulse energy of the difference frequency signal as in Fig. 8 for short delay times within the pump pulse duration (550 fs) using 150-fs injected pulses and a Kr pressure of 250 mbar. The pump pulse energies were 100 μJ (dotted line plus circles), 200 μJ (dashed line plus squares), and 450 μJ (solid line plus triangles). (b) Results of computer modeling of the resonant response of Kr with the pump pulse parameters $\tau_{\rm pl}=550$ fs, $W_1=100$ μJ (dots), 200 μJ (dashes), 450 μJ (solid line), and $p=250$ mbar and taking into account the Gaussian transverse beam profile. The corresponding values of the pump pulse rotation angle θ_1 at the beam axis are 2.3π, 4.6π, and 10.4π.

number of peaks increased with increasing pump pulse energy [Fig. 9(a)].

We explain these results by the model of two-photon resonant frequency mixing for pulses short compared to the polarization relaxation time (T_2') introduced in Sec. I. As will be shown below, the difference-frequency signal is proportional to the injected pulse intensity multiplied by a factor determined by the two-photon medium response. For the nonresonant Ar case, the medium response follows the pump pulse intensity quasistationarily. In the resonant case of Kr the two-photon response exhibits coherent Rabi oscillations which are observed within the pump pulse duration. The Rabi oscillations are followed by free relaxation of the excitation due to Doppler (T_D^*) and collisional (T_2') dephasing which occurs on a significantly larger time scale than the pump pulse duration τ_{pl} (see estimates below).

Using the theoretical approach developed in Sec. I, we now give a more quantitative explanation of the experimental data. The analysis can be simplified for the following reasons: First, experimentally the estimated two-photon absorption length at the pump pulse frequency considerably exceeds the active region length ($L_a\sim 1$ cm), so that propagation effects can be neglected; second, the intensities of the

injected and generated pulses are considerably lower than that of the pump pulse, and therefore the dynamics of the resonant interaction in both Ar and Kr is mainly determined by the pump pulse. Because no intermediate levels occur in Ar and Kr close to a one-photon resonance for the injected and the generated field-carrier frequencies, the phase velocity mismatch of the interacting fields is estimated to be not too large to affect the FWDFM process. Within the above approximations the temporal behavior of the generated field intensity is described by formula (11) in the limit of optically thin medium ($Gz \ll 1$):

$$|E_3(z,\tau)|^2 \propto |E_2(\tau-\Delta\tau)|^2 |\langle\sigma_{12}(\tau)\rangle|^2, \tag{36}$$

where $\Delta\tau$ accounts for the time delay of the injected pulse $E_2(\tau-\Delta\tau)$ with respect to the pump pulse field $E_1(\tau)$ centered at $\tau=0$. The macroscopic medium response $\langle\sigma_{12}\rangle$ is obtained by the averaging of σ_{12} over the Doppler line countour g: $\langle\sigma_{12}\rangle = \int g(\Delta\omega)\sigma_{12}(\Delta\omega)d\Delta\omega$. The Doppler dephasing time T_D^* in both gases is estimated to be $T_D^* \sim 100$ ps. When estimating T_2', we have to take into account that the highly excited upper resonant levels lie in the vicinity of the Rydberg states where the the collision cross section of an atom sharply increases. Using theoretical calculations [28], the cross section of a Kr atom excited to the upper resonant $6p$ level is estimated to be $\sigma = 10^{-12}$ cm^2. This leads to $T_2' \sim 10^3$ ps/p[mbar] due to the enlarged cross section and for gas pressures $p < 1$ bar the condition $\tau_{p1} < T_2'$ of cohererent interaction between the pump pulse and the two-photon transition is fulfilled. For the transition $4p^6\ {}^1S_0 \rightarrow 6p(5/2)_2$ in Kr, we have a resonant excitation since $|\Delta\omega| < \Delta\omega_1 \sim (\tau_{p1})^{-1}$. The analysis of spectroscopic data [26] shows that the energy difference between the resonant $6p(5/2)_2$ level and the nearest upper $6p(3/2)_1$ and lower $6p(1/2)_1$ lying levels allowed for two-photon excitation is about 200 cm^{-1} and exceeds both the pump pulse spectral width (55 cm^{-1}) and the dynamical Stark shift ($\Delta\omega_{\mathrm{St}} < 40$ cm^{-1}) of the resonant transition frequency. This justifies the accepted two-level model of laser-atom interaction.

Inserting solutions (30a) of the Bloch equations (3a) and (3b) into Eq. (36), we derive the following expression for the generated pulse intensity:

$$|E_3(\tau)|^2 \propto \frac{2\gamma^2[1-\cos\ \Psi_1(\tau)]+\sin^2\ \Psi_1(\tau)}{(1+\gamma^2)^2} \tag{37}$$

where the rotation angle $\Psi_1(\tau)$ is given by formula (30b).

Equation (37) shows that the measured signal as a function of τ is modulated with the Rabi frequency $\Omega_{\mathrm{Rabi}} = r_{12}(1+\gamma^2)^{1/2}|E_1(\tau)|^2/2\hbar$. Unlike the case of one-photon radiation-matter interaction (where the Rabi frequency is proportional to the amplitude $|E|$ of the resonant field [10]), in the two-photon coherent interaction case the Rabi frequency is quadratic in $|E_1|$. This means that the modulation frequency of the difference-frequency signal (37) increases linearly with the pump pulse intensity. At the time interval $\tau > \tau_{p1}$ the response relaxes according to $|\sigma_{12}(\tau)| \sim \exp(-\tau^2/T_D^2 - \tau/T_2')$ [15]. The fact that with an increase of gas pressure the decay time decreases (Fig. 8) indicates that collisional relaxation predominates. Using the measured dependence we estimated the collisional cross section by the value $\sigma \sim 2\times 10^{-12}$ cm^2.

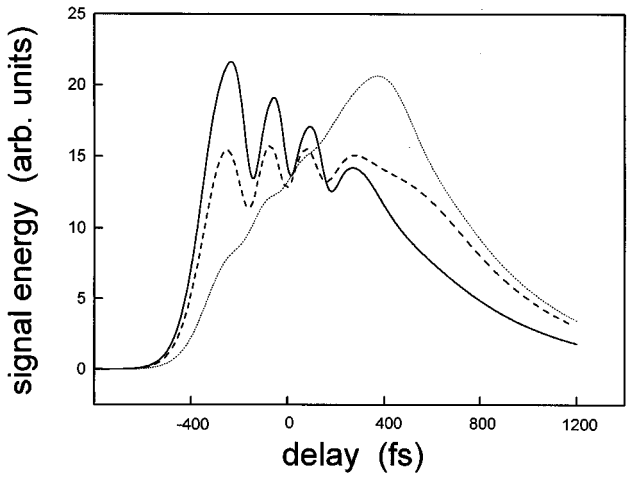

FIG. 10. Results of numerical modeling of the resonant response of Kr for different values of pump pulse frequency chirp: solid line, a bandwidth-limited sech-shaped pulse ($\Delta\nu_{pl}\tau_{pl}=0.31$) with the rotation angle at the beam axis $\theta_1 = 8\pi$; dashed line, a frequency-chirped pulse with the product $\Delta\nu_{pl}\tau_{pl}=1$; dotted line, a frequency-chirped pulse with the product $\Delta\nu_{pl}\tau_{pl}=3$.

In Fig. 9(b) we present the results of model calculations based on a numerical solution of the density-matrix equations for the resonant transition for a gas pressure $p = 250$ mbar (corresponding to $T_2' \approx 1.5$ ps) and pump pulse energies of 100, 200, and 450 μJ using two-photon transition parameters estimated from [26], $r_{12} = 2.1\times 10^{-24}$ cm^3 and $\alpha_{11} - \alpha_{22} = 5.8\times 10^{-24}$ cm^3, and taking into account the transverse beam profile. The results are in qualitative agreement with the measured data and show that the effect of a finite temporal resolution as well as the relaxation processes flatten the modulations of the atomic response. Even for pulses with a maximum energy of 450 μJ the field-induced broadening due to fast Rabi oscillations was still smaller (~ 150 cm^{-1}) than the energy separation between the upper neighboring levels. The validity of the two-level model is supported by the fact that even in this extreme regime the characteristic oscillating structure appeared experimentally only within the interaction time. There was no signal modulation at the stage of free relaxation of the excitation, which would indicate the excitation of other levels.

The effects of atomic coherency are rather sensitive to the influence of phase modulation of applied laser field. We have numerically studied the dynamics of the resonant response of Kr for different values of the pump pulse frequency chirp (Fig. 10). As can be seen from Fig. 10, when the pump pulse has a frequency chirp such that the bandwidth product ($\Delta\nu_1\tau_{p1}$) is close to 1 the atomic response still shows temporal oscillations characteristic of Rabi nutations of atomic populations. However, starting from $\Delta\nu_1\tau_{p1} \geqslant 3$ the oscillating features completely disappear, and the temporal behavior of the response rather corresponds to the case of off-resonant radiation-atom interaction.

We have found that the critical energy density for the observation of Rabi oscillations in our case ($\gamma > 1$) is determined by the requirement that the Rabi angle $\theta_1 = \Psi_1(\infty)$

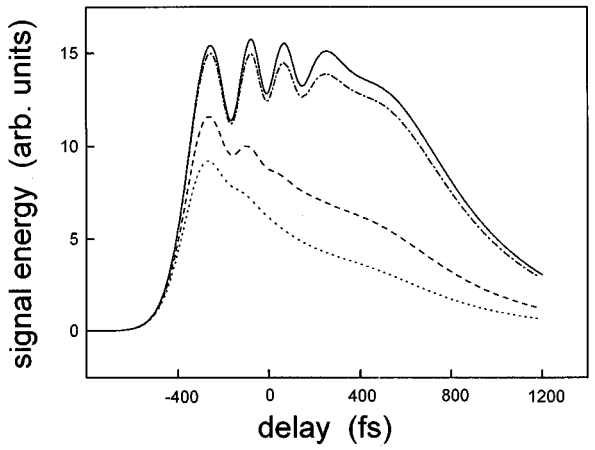

FIG. 11. The influence of one-photon ionization from the upper resonant level on the dynamics of the resonant response of Kr: solid line, $\sigma_i=0$ (without photoionization); dashed-dotted line, $\sigma_i=3\times10^{-19}$ cm^2; dashed line, $\sigma_i=3\times10^{-18}$ cm^2; dotted line, $\sigma_i=10^{-17}$ cm^2. The pump pulse energy $W_1=350$ μJ.

[see Eq. 30(b)] at the beam axis must exceed the value $\theta_1=2\pi$. As can be seen qualitatively from Eq. (37), in this situation the population difference and the response σ_{12} make one complete oscillation. The corresponding pump pulse critical fluence was calculated to be 0.35 J/cm^2, which is also in good agreement with our observations.

The influence of one-photon ionization of the upper resonant level by the pump radiation on the FWDFM process has been also analyzed. In the presence of photoionization the density-matrix equation for the upper level population σ_{22} contains an intensity-dependent relaxation term accounting for the depletion of the level with the rate $w_i=1/T_i=\sigma_i I_1/h\omega_1$ (where σ_i is the photoionization cross section, and I_1 is the pump pulse intensity). The equation for the nondiagonal element σ_{12} has an additional term describing the ionization-induced line broadening $\Gamma_i=w_i/2$. Because of the lack of reliable data on ionization cross section of the $6p(5/2)_2$ level of the Kr atom with radiation at $\lambda_1=193$ nm, we have carried out model calculations of the medium response with the values of σ_i varying in the range 10^{-19}–10^{-17} cm^2. It has been found (see Fig. 11) that the oscillating structure of the coherent response is still well defined for $\sigma_i<3\times10^{-19}$ cm^2, but completely desappears due to the ionization-induced relaxation process for $\sigma_i>5\times10^{-18}$ cm^2. From these model calculations we have estimated the ionization cross section to be of the order of $\sigma_i\approx1.5\times10^{-19}$ cm^2. This means that for the pump pulse intensities used (~1 TW/cm^2), the photoionization time of the atom is $T_i=1/w_i\approx10$ ps and still long enough compared to the pulse duration (~0.5 ps) and the collisional relaxation time (~1.5 ps). The pump pulse energy density required to completely ionize the atom from the excited state can be estimated to be $W_i\approx10$ J/cm^2, that is, an order of magnitude higher than the energy densities used in the discussed resonant experiment. Our analysis thus shows that the effects of saturation of resonant frequency conversion due to photoionization of the medium will be important for the pump pulse energy densities $W\geqslant10$ J/cm^2.

CONCLUSION

The results of a theoretical and experimental study of the FWDFM process under the condition of two-photon resonant and quasiresonant interaction of femtosecond pulses with atomic media have been presented. Particular attention was paid to the facts that the experimentally used intense femtosecond pulses have durations comparable to and even shorter than the polarization relaxation time of the medium, and that effects of two-photon coherent laser-atom interaction have an important role in the difference-frequency vuv field generation.

To describe adequately the real experimental situation and interpret nonstationary resonant and quasiresonant phenomena involved in the FWDFM process, a theoretical model based on a self-consistent solution of the Bloch equations for the resonant atomic transition and the Maxwell equations for the fields has been developed. The model makes it possible to investigate frequency conversion at the stage when the effects of saturation of the nonlinear polarization dominate, and to estimate the maximum conversion efficiency for difference-frequency generation. It was found that the effect of interference of the contributions of two processes, two-photon absorption at ω_1 and two-photon emission at ω_2 and ω_3, imposes principal limitations on the maximum achievable efficiency in the FWDFM process. As a result, the efficiency of energy transformation from the pump to the vuv field is saturated even under perfect phase-matching conditions. The larger the cross section for the FWDFM process, the smaller the vuv field saturation energy. Therefore, operation in rather close resonance with intermediate atomic states can lead to a reduction of the conversion efficiency that is supported by our experimental observation in Ar. Our estimations show that an optimized FWDFM process can provide a vuv field generation with efficiencies up to several tens of percent. The approach has also been applied to a modeling of the FWDFM process under conditions of coherent resonant interaction, taking into account the nonlinear absorption of the fields in the medium. The maximum achievable conversion efficiency here is limited mainly by the coherent propagation effects and by a formation of a 2π pulse of self-induced transparency. It is interesting that in the coherent interaction regime the vuv field is produced in a form of femtosecond pulses with durations considerably shorter than the durations of both the input pump and injected pulses.

Experimentally, we developed a vuv femtosecond laser source tunable in the range 102–124 nm based on FWDFM of intense femtosecond ArF pulses and synchronized injection pulses tunable in the visible and near infrared. The system has the potential to extend the tuning range across nearly the whole vuv (96–190 nm) by up-converting the injection pulses into the ultraviolet spectral region or extending them to the IR. Further improvement of the conversion efficiency should be possible by employing a pulsed gas jet in order to obtain phase matching and to avoid spatial and temporal distortions of the pump beam due to self-action and to minimize losses for the vuv radiation caused by absorption in long gas paths.

We have also demonstrated that the femtosecond-pulse FWDFM-process makes it possible to study the coherent dy-

namics of a quantum transition in an intense resonant field. With this technique, the two-photon resonant response of atomic Ar and Kr excited by an intense uv pulse with a duration short compared to the polarization relaxation time was investigated. In Ar the frequency detuning from the two-photon transition is sufficiently large, and the response of the medium shows quasistationary behavior determined by the instant value of the pump pulse field. In the resonant Kr case coherent two-photon Rabi oscillations and subsequent free relaxation of the excitation have been observed. To our knowledge, these results are the first direct experimental observation of the coherence induced by a two-photon excitation of an atomic by femtosecond vuv pulses. The measured difference frequency probes the squared amplitude of the off-diagonal matrix element of the transition. Such information about the dynamics of quantum transitions is of importance for controlling and optimizing such processes as two-photon resonance frequency conversion and harmonic generation, as well as time-resolved studies of Rydberg states in atoms and molecules.

[1] R. E. Walkup, J. A. Misewich, J. H. Glownia, and P. P. Sorokin, J. Chem. Phys. **94**, 3389 (1991).
[2] F. Seifert, J. Ringling, F. Noak, V. Petrov, and O. Kittelmann, Opt. Lett. **19**, 1538 (1994).
[3] G. Hilber, A. Lago, and R. Wallenstein, J. Opt. Soc. Am. B **4**, 1753 (1987).
[4] G. C. Bjorklund, IEEE J. Quantum Electron. **QE-11**, 287 (1975).
[5] J. F. Reintjes, *Nonlinear Optical Parametric Processes in Liquids and Gases* (Academic, New York, 1984).
[6] J. H. Glownia, D. R. Gnass, and P. P. Sorokin, J. Opt. Soc. Am. B **11**, 2427 (1994).
[7] A. Tünnermann, C. Momma, K. Mossavi, C. Windolph, and B. Wellegehausen, IEEE J. Quantum Electron. **29**, 1233 (1993).
[8] A. Tünnermann, K. Mossavi, and B. Wellegehausen, Phys. Rev. A **46**, 2707 (1992).
[9] O. Kittelmann, J. Ringling, A. Nazarkin, G. Korn, and I. V. Hertel, Phys. Rev. Lett. **76**, 2682 (1996).
[10] L. Allen and J. H. Eberly, *Optical Resonance and Two-Level Atoms* (Wiley, New York, 1975).
[11] E. M. Belenov and I. A. Poluektov, Zh. Eksp. Teor. Fiz. **56**, 1407 (1969) [Sov. Phys. JETP **29**, 754 (1969)].
[12] J.-C. Diels and A. T. Georges, Phys. Rev. A **19**, 1589 (1979).
[13] I. A. Poluektov and A. Nazarkin, Kvant. Electron. (Moscow) **6**, 2525 (1979) [Sov. J. Quantum Electron. **9**, 1495 (1979)].
[14] F. Vallee, F. Bogani, and C. Flytzanis, Phys. Rev. Lett. **66**, 1509 (1991).
[15] C. S. Mullin, D. Kim, M. B. Feller, and Y. R. Shen, Phys. Rev. Lett. **74**, 2678 (1995).
[16] D. C. Hanna, M. A. Yuratich, and D. Cotter, *Nonlinear Optics of Free Atoms and Molecules* (Springer-Verlag, Berlin, 1979).
[17] Y. R. Shen, *The Principles of Nonlinear Optics* (Wiley, New York, 1984).
[18] N. P. Garayantz, V. S. Grigoryan, S. A. Michaelian, K. B. Petrossian, and K. M. Pokhsrarian, J. Mod. Opt. **38**, 591 (1991).
[19] D. Grischkowsky, M. M. T. Loy, and P. F. Liao, Phys. Rev. A **12**, 2514 (1975).
[20] J. V. Rudd, G. Korn, S. Kane, J. Squier, G. Mourou, and P. Bado, Opt. Lett. **18**, 2044 (1993).
[21] J. Ringling, O. Kittelmann, F. Noak, G. Korn, and J. Squier, Opt. Lett. **18**, 2035 (1993).
[22] J. Ringling, O. Kittelmann, F. Noak, U. Stamm, J. Kleinschmidt, and F. Voss, Opt. Lett. **19**, 1639 (1993).
[23] S. R. Greenfield and M. R. Wasielewski, Opt. Lett. **20**, 1394 (1995).
[24] V. Petrov, F. Seifert, O. Kittelmann, J. Ringling, and F. Noack, J. Appl. Phys. **76**, 7704 (1994).
[25] R. Mahon, T. J. McIlrath, V. P. Meyerscough, and D. W. Koopman, IEEE J. Quantum Electron. **QE-15**, 444 (1979).
[26] M. Aymar and M. Coulombe, At. Data Nucl. Data Tables **21**, 537 (1978).
[27] N. Tan-no, K. Yokoto, and H. Inaba, Phys. Rev. Lett. **29**, 1211 (1972).
[28] E. W. McDaniel, J. B. A. Mitchell, and M. E. Rudd, *Atomic Collisions: Heavy Particles Projectiles* (Wiley, New York, 1993).